Nuclear Materials and Energy 25 (2020) 100859

Contents lists available at ScienceDirect

Nuclear Materials and Energy

journal homepage: www.elsevier.com/locate/nme

Erosion and screening of tungsten during inter/intra-ELM periods in the JET-ILW divertor

A. Huber [a,*], S. Brezinsek [a], V. Huber [b], M. Sertoli [c], G. Sergienko [a], I. Borodkina [d], M. Baruzzo [e], A. Kirschner [a], D. Borodin [a], J. Mailloux [f], S. Aleiferis [g], P. Carvalho [h], K. Lawson [f], Ch. Linsmeier [a], A. Meigs [f], S. Menmuir [f], Ph. Mertens [a], E. Pawelec [i], A. Shaw [f,1], JET contributors

[a] Forschungszentrum Jülich GmbH, Institut für Energie- und Klimaforschung - Plasmaphysik, 52425 Jülich, Germany
[b] Forschungszentrum Jülich GmbH, Supercomputing Centre, 52425 Jülich, Germany
[c] Max-Planck-Institut fur Plasmaphysik, D-85748 Garching, Germany
[d] Institute of Plasma Physics of the CAS, Prague, Czech Republic
[e] Consorzio RFX, Corso Stati Uniti 4, 35127 Padova, Italy
[f] CCFE, Culham Science Centre, Abingdon OX14 3DB, UK
[g] NCSR 'Demokritos' 153 10, Agia Paraskevi Attikis, Greece
[h] Instituto de Plasmas e Fusão Nuclear, Instituto Superior Técnico, Universidade de Lisboa, Portugal
[i] Institute of Physics, University of Opole, Oleska 48, 45-052 Opole, Poland

ARTICLE INFO

Keywords:
Tungsten erosion
Divertor screening of tungsten
Tungsten imaging spectroscopy
W Divertor
JET-ILW
PSI
PFC

ABSTRACT

Intra-ELM tungsten sources, which dominate the total W source, are quantified in the inner and outer divertor of JET-ILW. The amount of the sputtered W atoms for individual ELMs demonstrates a clear dependence on the ELM frequency. It decreases when the pedestal temperature is lower and, correspondingly, the ELM frequency is higher. Nevertheless, the entire gross erosion W source (the number of eroded W atoms per second due to ELMs) increases initially with ELM frequency and reaches its maximum at $f_{ELM} \approx$ 50–55 Hz followed by its reduction in the high frequency range.

The in/out asymmetry of the intra-ELM W sources during ELMs is a critical issue and is investigated in this contribution. At a lower ELM frequency of about 35 Hz the outer divertor gross W source is larger by a factor of 1.5. However the in/out asymmetry of the W erosion decreases strongly with ELM frequency demonstrating a nearly symmetric W source in both divertor legs at frequencies above 70 Hz. The screening of tungsten in the open magnetic configuration with strike points on tile 5 is more efficient by a factor of about 1.7 than in the corner configuration with the outer strike point at the pumping duct entrance.

1. Introduction

Tungsten (W) is intended as the main plasma-facing material (PFM) in fusion devices such as the divertor of ITER because of its high threshold energy for sputtering, a high melting point and a low tritium inventory. The net erosion of W can significantly limit the lifetime of the respective wall components while the influx of W into the confined region can result in a dilution of the fusion plasma and additional energy losses due to radiation. In fact, the interplay of the W source strength, the screening of W by the divertor geometry/plasma and the transport of W in the plasma determines the W content in the plasma core and hence affects the plasma performance [1]. Therefore, it is essential to get a complete understanding of the interplay between the gross erosion source of W and its screening to find the recipe to control the net W source and minimize the impact of eroded W on the confined plasma.

In particular, the knowledge of the W-erosion sources in the divertor regions, outer as well as inner, is very important. Typically, the W erosion source in present fusion devices is measured in-situ by optical spectroscopy of the tungsten line emission, a method which concentrates mainly on the W erosion measurements in the outer divertor leg [2,3,4]. On the other hand, the determination of the W sources is very challenging in the inner divertor area because the relatively weak line

* Corresponding author.
E-mail address: a.huber@fz-juelich.de (A. Huber).
[1] See the author list of E. Joffrin et al. accepted for publication in Nuclear Fusion Special issue 2019, https://doi.org/10.1088/1741-4326/ab2276.

https://doi.org/10.1016/j.nme.2020.100859
Received 18 August 2020; Received in revised form 30 October 2020; Accepted 23 November 2020
Available online 30 November 2020

radiation emitted by neutral tungsten is often masked by the presence of the plasma continuum radiation (free-free, free-bound and molecular ionisation continuum) and thermal radiation from the hot surfaces [5]. For this reason, the W source in the inner divertor has not yet been investigated, and it was assumed that this source is negligible compared to the source in the outer divertor. Therefore a strong in/out asymmetry in the W erosion source is usually assumed.

In this work, an analysis of the gross erosion of tungsten during inter/intra-ELM periods in the JET-ILW divertor legs, inner and outer, is presented and discussed. For the subtraction of the continuum radiation, several approaches were developed and used to evaluate the W erosion in the inner as well as in the outer divertor area. The determined W sources demonstrate a strong dependence on the pedestal electron temperature and, correspondingly, on the ELM frequency. The in/out asymmetry of the intra-ELM W sources during ELMs is a critical issue and is investigated in this contribution. It will demonstrated that the contribution of the inner divertor region to the total W source is significant and cannot be neglected. Especially in the large ELM frequency range in which the asymmetry disappears and the inner and outer erosion rates are almost identical.

Additionally, an analysis of the divertor screening of tungsten during inter/intra-ELM periods in the JET-ILW divertor will be presented and discussed for different magnetic field shapes: open and closed divertor configuration (corner configuration). Note that the corner configuration is intended as a reference shape for scenarios of the deuterium–tritium experiments on JET scheduled for 2021.

2. Methods for evaluation of W erosion in the JET-ILW divertor

Tungsten erosion is assessed in-situ by passive emission spectroscopy of the tungsten emission. This mainly involves the observation of the most prominent WI transition ($5d^5(^6S)6s\ ^7S_3 \rightarrow 5d^5(^6S)6p\ ^7P^o_4$) at $\lambda = 400.9\ nm$ of the sputtered W atoms in order to determine the gross erosion. On JET-ILW, several spectroscopic systems are used to monitor the WI line radiation:

- The mirror-linked divertor spectroscopy system on JET (we will refer in this contribution to the KT3 diagnostic) [6,7] affords spatially resolved measurements of the plasma emission in 22 lines-of-sight (LOS) covering 320 mm of the outer divertor. Each LOS has a toroidal dimension of 2 mm and a poloidal size of 14.5 mm at the divertor targets. With three Czerny-Turner spectrometers, it covers a spectral range of 200–1100 nm with a range of grating options that offer flexibility in the selection of the wavelength window and the spectral resolution. This spectrally resolved measurement with exposure times of 40 ms permits fine background subtraction and spectral profile study.
- The W filterscope diagnostics [8] with a circular lines of sight with a diameter of 380 mm each covers the entire inner and outer divertor. The collected W I emission light is transmitted via fibre optics to Photo Multiplier Tubes (PMTs), which are equipped with 400.9 nm band pass filters (≈1nm of Full Width at Half Maximum (FWHM)) and offer a time response of up to 10 kHz.
- A mirror-based endoscope system [5,9,10] is equipped with an imaging system of four digital monochrome CCD cameras (AVT Pike F-100B fibre), each combined with filter wheels for narrow-band interference and neutral density filters. Cameras can operate at a full frame rate of 32.8 Hz (16bits) (or 59.9 Hz with reduced dynamic range (8bit)). These cameras have a high spatial resolution, that is ≤2 mm at the divertor targets. In this contribution, two cameras equipped with image intensifiers were used with identical two-dimensional views and with interference filters of different bandwidths centred on the W I (400.88 nm) emission line installed in front of the image intensifier photocathode.

In ELMy H-mode operation scenario under completely attached divertor conditions, both phases (the intra- and the inter-ELM phase) contribute to the gross erosion of tungsten. Distinguishing the tungsten erosion between these two phases is challenging in particular at high ELM frequencies because the temporal resolution of the diagnostics is often not sufficient to separate the intra- and inter-ELM phases. At ELM frequency, f_{ELM}, below 25 Hz, the mirror-linked divertor spectroscopy system KT3 can clearly separate the inter- and intra-ELM phases in the outer director. However, this will severely limit the analysis to a low f_{ELM} region. The imaging spectroscopy system (KL11) with a new algorithm for the subtraction of the continuum radiation can distinguish these phases at $f_{ELM} < 60$ Hz in the inner as well as outer divertor area. The fast PMT system for the photon flux density measurements, I_W [Ph/(s m^2 sr)], is an excellent tool for the analysis of the W erosion during the Intra-ELM phases. However, because of the usage of a filter with FWHM of 1 nm, the PMT signals are overestimated due to the contribution of the plasma continuum [4].

In the present article, three approaches are chosen to provide a quantitative measure for the W-erosion and to distinguish the erosion source in the intra- and the inter-ELM phases:

I. The combination of two spectroscopic systems, KT3 and PMT, with good spectral and temporal resolution, respectively, can separate both contributions. This is an identical approach to the one described and used in the previous work [4]. This method enables the calculation of the background continuum intensity when comparing the photon fluxes of these two diagnostics during the flat top phases of the discharges, as shown in Fig. 1. For comparison, the PMT signal is integrated over the time window that corresponds to the time exposure of KT3 spectroscopy (40 ms). Additionally, to match the PMT spatial resolution, the weighting of the KT3 channels is performed. Fig. 1 shows the linear dependence between PMT and KT3 signals with a clear offset in the PMT measurements. This offset is due to the plasma continuum with the main contribution of the bremsstrahlung. The plasma continuum values are of about 7.75×10^{16} ph/(s m^2 sr). Assuming the ELM duration of approximately $\tau_{ELM} = 0.5$–1.0 ms and continuum emission is not changing during the ELM, the contribution of the plasma continuum to the signal during the ELM is about 3.9–7.75×10^{13} ph m^{-2} sr^{-1}.

II. In the second approach we calculate the accumulated photon flux, $\int I_W dt$, instead of the instantaneous photon flux. In this case, we maintain the original temporal resolution of the raw data, at the same time reducing the noise in the data. During the stationary phases with constant absorbed power, constant erosion rate and constant plasma continuum, the accumulated photon flux raises with a constant slope over several tens of milliseconds, which can easily be determined. This slope is determined by plasma continuum as well as the photon fluxes from the W sputtered atoms during the inter-ELM time window. Fig. 2 shows time traces of PMT photon fluxes, I_W, and the accumulated photon flux , $\int I_W dt$, collected from the inner and outer divertor regions. During an ELM event, however, there is a jump in the accumulated photon flux. The height of this jump corresponds to the radiated WI photons (per unit area and per unit solid angle) during the ELM. Fig. 2 demonstrates jumps of about 5.8×10^{14} ph m^{-2} sr^{-1} and 3.9×10^{14} ph m^{-2} sr^{-1} for the outer and inner divertors, respectively. The number of radiated W I photons during the ELM is factor of 7.25–14.5 larger than the number of photons originating from the plasma continuum. Assuming that the continuum plasma background during the ELM is the same as during the inter-ELM phase, the number of atoms sputtered due to the ELM event can be clearly separated from the eroded ones during the inter-ELM phase. Approach (III) discussed next does not use the assumption about the continuum. A cross comparison of the approaches (II) with the approach (III) shows a good

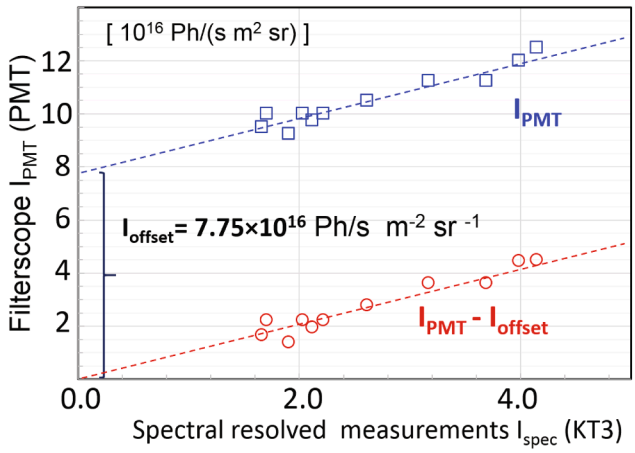

Fig. 1. Linear dependence between PMT and KT3 signals with a clear offset in the PMT measurements. This offset is due to the plasma continuum with the main contribution of the Bremsstrahlung.

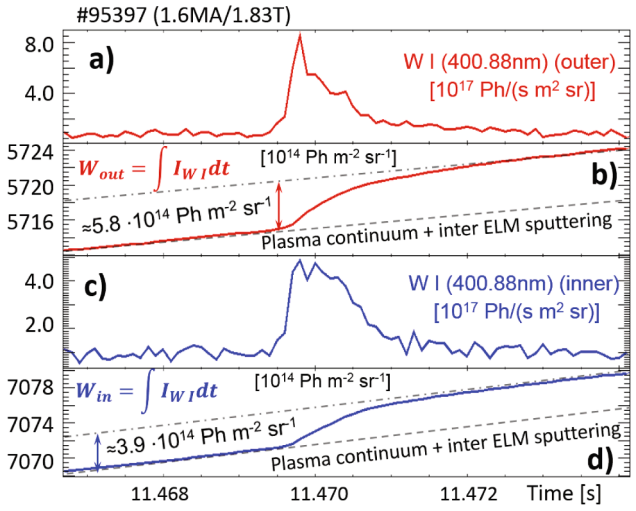

Fig. 2. Time traces of the WI photon flux density in the outer (a) and inner (c) divertor regions, the accumulated photon flux, $\int I_W dt$, in the outer (b) and inner (d) divertor.

agreement within 10% and therefore confirms the correctness of the assumption that the continuum plasma background during the ELM is the same as during the inter-ELM phase. The approach (II) can be used for the determination of the sputtered particle fluxes in the outer as well as in the inner divertor.

III. Spectroscopic imaging with the help of two digital cameras with the same two-dimensional view, equipped with interference filters of different bandwidths centred on the W I (400.88 nm) emission line. A new method for the subtraction of the continuum radiation for the JET imaging system was successfully developed and is now used to evaluate the W erosion even in the inner divertor region [5] where the strong recombination emission is dominating over the tungsten emission.

Good agreement between the mentioned approaches was found.

The measured photon fluxes are converted into particle fluxes by applying inverse photon efficiencies according to the multi-machine scaling law [2,11,12]:

$$\Gamma_W = 4\pi \frac{S}{XB}(T_e) \cdot I_{WI} \quad (1)$$

$$S/XB(T_e) = 53.63 - 56.07 \times e^{(-0.045 \times T_e[eV])} \quad (2)$$

where I_{WI} is the measured photon flux density of the WI emission line and the S/XB multiplication factor is the so-called inverse photon efficiency or the number of ionizations per photon.

This multi-machine S/XB scaling for WI emission [2,11,12] without electron density dependence was developed taking into account experimental data from TEXTOR, ASDEX Upgrade, PSI and PISCES. Note that the S/XB values for the larger electron temperature represent data from TEXTOR measured at electron densities n_e between 2.0×10^{18} m^{-3} and 1.0×10^{19} m^{-3}. This multi-machine fit reproduces well the shape of the corresponding theoretical curve of S/XB for WI emission line at 400.9 nm deduced from the ADAS database [13]. However ADAS modelling predicts higher S/XB coefficients at higher electrons densities. The most likely reason for the discrepancy are not the electron impact excitation rate coefficients used in ADAS, but the ionisation rate coefficients for W. The experimentally determined ionisation rates revealed a discrepancy when compared with theoretical calculations (ADAS, GKU, and Lotz) [11,12]. Nevertheless, the electron density dependence of the S/XB coefficient has been observed recently by studies in DIII-D at high plasma densities [14]. The DIII-D experiments demonstrate the increase of the WI S/XB coefficients for densities above 10^{19} m^{-3}. Therefore, the electron density dependence of the WI S/XB values may become important. It is important for the calculation of the W erosion during the ELMs in particular, where the density is probably higher than 1.0×10^{19} m^{-3} [15]. Nevertheless, studies of the electron density dependence of the WI S/XB coefficient are outside the scope of this contribution. Further studies are required to resolve this issue. In this work the multi-machine fit for WI S/XB is used and thus the S/XB coefficient may be underestimated.

The S/XB values for the inter-ELM phases are determined by the electron temperature, which is measured by an array of Langmuir probes in the divertor region. During the ELMs, an electron temperature of 70–100 eV at the strike point is assumed, which gives S/XB values of about 50 according to the multi-machine scaling [2,11,12]. Note that the S/XB values in the temperature range between 50 eV and 200 eV are only weakly dependent on T_e: they increase from 48 to 53.6. Therefore, the particle flow calculation is not sensitive to our assumption of $S/XB =$ 50. Quite similar values for S /XB for the intra-ELM phases have been used in [1,4,20]. This enables a direct comparison of the W erosion results with these earlier works.

3. Experimental results

3.1. Erosion of tungsten during inter/intra-ELM periods

In this section, the Type I H-mode plasmas with a toroidal magnetic field, $B_t = 1.83$ T and plasma current, $I_p = 1.6$ MA, $q_{95} \approx 3.6$ at a low triangularity configuration ($\delta_{av} \approx 0.23$) are investigated. The divertor geometry of the chosen configuration has the inner strike on the inner vertical divertor target and the outer strike on the horizontal divertor target (bulk W tile 5) as shown in Fig. 5a (shape A). The auxiliary heating powers, NBI and ICRH, were 12.5–13 MW and 1.2–1.4 MW respectively to maintain the plasma stored energy (W_{dia}) at the level of 2.6–2.8 MJ. It is known that the simplest and most reliable method for increasing the ELM frequency is gas injection. Experience shows that the ELM frequency increases strongly with increased gas injection [16,17]. At the same time, gas fuelling affects the plasma, the plasma energy confinement and the pedestal temperature $T_{e,ped}$. As shown in [17], a low (high) gas fuelling rate correlates with a higher (lower) $T_{e,ped}$ and higher (lower) energy confinement in JET-ILW plasmas. In this work, respective scans have been performed over a deuterium fuelling range of 3.5×10^{21}el/s-6.8×10^{21} el/s with constant input heating power to study the impact of the ELM size and ELM frequency on the W erosion.

Fig. 3 shows the number of sputtered W atoms as function of the ELM frequency. Here the total number of W atoms in the outer (inner) divertor area is integrated over the entire outer (inner) strike point. The discharges with low fuelling rates corresponds to the large ELMs and correspondingly to the lower ELM frequencies. The strength of ELMs can be derived from the loss of stored plasma energy, the so-called ELM energy losses E_{ELM}. Analysis of Type I ELMs [18] shows that ELM energy losses are correlated with the density and temperature of the pedestal plasma before the ELM crash. With an increase of the ELM frequency the loss in stored plasma energy during the ELM, the ELM energy loss (E_{ELM}) as well as the ELM size decreases because the ELM size, E_{ELM}, is inversely proportional to the ELM frequency f_{ELM} [19] ($E_{ELM} \sim 1/f_{ELM}$).

One sees that the amount of sputtered W atoms for individual ELMs

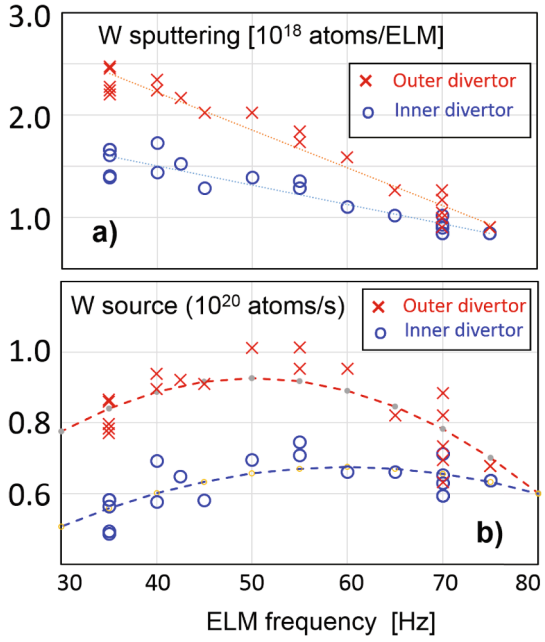

Fig. 3. a) The number of the sputtered W atoms per single ELM in the inner/outer divertor legs and (b) the outer/inner divertor tungsten source as function of the ELM frequency. The ELM frequency scan was performed with a constant input heating power by varying the gas refuelling rate from 3.5×10^{21} el/s to 6.8×10^{21} el/s.

demonstrates a clear dependence on the ELM frequency. It decreases when the pedestal temperature is lower and, correspondingly, the ELM frequency is higher. However, when we talk about the entire gross erosion W source (the number of eroded W atoms per second due to ELMs), an increased ELM frequency up to $f_{ELM} = 50$–55 Hz results in an increased W source as shown in Fig. 3b. Beyond 55 Hz there is an opposite tendency for the source to descend in both the inner and outer divertor regions. This roll-over in total W erosion source with increasing ELM frequency is consistent with previously published results on JET [4] as well as on DIII machine [20]. The total intra-ELM W source in the outer divertor varies in the observed frequency range between 0.8×10^{20} atoms/s and 1.0×10^{20} atoms/s. Based on the fast PMT measurement, the inter-ELM induced sputtering amounts to $(1.0–1.1) \times 10^{19}$ atoms/s integrated over the entire outer strike point. Based on T_e probe measurements of 12 eV at the outer strike point, the *S/XB* value of 21 is used here according to the multi-machine scaling [2,11,12]. Thus, the intra-ELM sputtering dominates by a factor of 7–10 over inter-ELM sputtering in the entire range of ELM frequency, a finding which is fully in line with previous observations [1,2,5].

In JET-ILW it was shown that the dominant W erosion mechanism in the divertor at $T_e = 10$–20 eV during the inter-ELM phase is due to beryllium impurities [2,4]. However, tungsten sputtering becomes important during ELMs and even dominates due to deuterium [21]. According to the free streaming model [22], the electrons transfer during the ELMs on the way to the divertor target their parallel energy to ions to maintain quasi-neutrality. It is experimentally observed in type I H-mode discharges that the maximum sum of the ion and electron energy linearly depends on the pedestal electron temperature: $\max(E_i + E_e) = 5.23 \times T_{e,ped}$ [23]. The model assumes that only $E_{e,\perp}$ is left in E_e, resulting in almost mono-energetic ions with $E_{i,\max}$ up to $4.23 \times T_{e,ped}$.

An analytical model developed by Borodkina et al. in [24] for the interpretation of the Langmuir Probe measurements and for estimation of the W sputtered influx describes well the intra-ELM sputtering source as a function of the pedestal temperature ($T_{e,ped}$). Taking into the account the pedestal temperature drop during ELM, the average incident energy of ions, $< E_i >$ is lower than $E_{i,\max} = 4.23 \times T_{e,ped}$. As is shown in [24] the $< E_i >$ energy is around 1.3 keV for pedestal temperature prior to the ELM event of $T_{e,ped}^{max} = 500$ eV. In our fuelling scan the $T_{e,ped}$ varies from 380 eV to 670 eV, which corresponds to the variation in $E_{i,\max}$ energy of impinging ions from 1.7 to 2.83 keV (the average incident energy of ions ≈1–2 keV) . The sputtering yields for W by different deuterium and beryllium ions begin to flatten at higher energies above 3 keV [25]. For the incident energy of ions in the energy range between 1 keV and 2 keV, however, the sputtering yield decreases with increasing of the fuelling rate (ELM frequency) due to decreasing of the $T_{e,ped}$: a reduction by factors of 1.5 and 1.2 in the yield due the deuterium and beryllium ions, respectively. Additionally, the W influx during the high frequency ELMs is decreased due to the reduction in the ion fluxes to the target, $J_{sat.ELM}$, by a factor of 1.1–1.25 as measured by LPs. Both the reduction in yield as well as in ion fluxes lead to the reduced ELM-induced W sputtering by a factor of 1.7–1.9 which is in line with the observed reduction in the amount of sputtered W atoms for individual ELMs with ELM frequency f_{ELM} : a factor 2.0–2.3 in the outer and 1.7 in the inner divertor area.

Fig. 3 shows that the contribution of the inner divertor region to the total W source is significant and cannot be neglected. However this contribution strongly depends on the ELM frequencies. Therefore, the in/out asymmetry of the intra-ELM W sources during ELMs is a critical issue and is investigated in this contribution. At a lower ELM frequency of about 35 Hz the outer divertor gross W source is larger by a factor of 1.5. But the in/out asymmetry of the W erosion decreases strongly with ELM frequency, demonstrating a nearly symmetric W source in both divertor legs at frequencies above 70–80 Hz. The physics of asymmetric W erosion is very complex and detailed modelling is required to fully understand it.

3.2. Screening of tungsten sources in the JET-ILW divertor

W screening in the divertor is defined as the fraction of eroded tungsten, S_W, that reaches the last closed flux surface (LCFS). Higher (lower) S_W values indicate that more (or less) tungsten reaches the plasma core and that the screening is correspondingly poorer (or better). The product of S_W and Γ_W, the total number of eroded W particles, $\Phi_{in} = S_W\Gamma_W$ is the inward particle flux into the main plasma which impacts the evolution of the core W density. The fraction S_W is determined by the diffusion and convection of W ions in the SOL which is in competition with parallel ion motion towards the divertor targets. The last one is defined by the balance between the thermal force, F_{therm}, and the friction force, F_{fric}, along magnetic field lines [26]. The thermal force, induced by the ion and electron temperature gradient, pushes the impurity ions up the temperature gradients, $dT_{e,i}/dl$ to the main plasma (core-SOL plasma boundary). On the other hand, the frictional force, caused by the plasma flow from the main plasma to the divertor plates, acts on the impurity ions in the direction parallel to the magnetic field lines to the divertor area. Additionally, when sputtered W atoms are ionized in the vicinity of the divertor and the penetration depth of the neutrals becomes as small as the ion Larmor radius, local redeposition is likely to occur within the first gyration of the W ion. This effect is called prompt-redeposition [27]. For the divertor plasma conditions up to 90% of the sputtered W atoms could be promptly redeposited [28,29]. In the recent article [21] redeposition values up to 99% are predicted by numerical simulations for the plasma with $I_p = 2.5$MA, $B_t = 2.7$ T with an electron density of 5×10^{19} m^{-3} at the strike point and electron temperatures between 10 and 30 eV. However, it depends strongly on the electron density at the strike point and the toroidal magnetic field as well as on the balance between the thermal force, F_{therm}, and the friction force, F_{fric}, along magnetic field lines. As reported in [21] smaller deposition values are simulated with reduced electron density. The thermal force can also reduce tungsten deposition, but an ion temperature gradient of about 0.1 eV/mm or more is required for a significant effect. redeposition value of about 91.7% is predicted for an ion temperature gradient of 0.1 eV/mm [21]. Therefore the W net erosion as well as the S_W could significantly be reduced due to the prompt-redeposition effect.

The expression for the screening factor, S_W, can be evaluated by the following particle balance equation:

$$\frac{dN_W}{dt} = \Phi_{in} - \Phi_{out} = S_W\Gamma_W - N_W/\tau_W \quad (3)$$

where $\Phi_{out} = N_W/\tau_W$ is the outward particle flux from the main plasma, τ_W is the global W particle confinement time, Γ_W is the total number of the gross eroded W particles per time unit of a second (W source). Γ_W also includes the atoms, which are promptly redeposited. In the steady-state condition, $t \gg \tau_W$, the left term in the equation (3) can be neglected and one obtains the expression of W screening factor in the divertor:

$$S_W = N_W/(\tau_W\Gamma_W) \quad (4)$$

Dedicated H-mode experiments have been carried out at JET with the ITER-like wall (JET-ILW) to study the impact of plasma configurations on S_W in the divertor. In this contribution, Type I ELMy H-mode plasmas at $B_T = 2.5$ T, $I_p = 2.3$ MA have been examined in single null plasma discharges in deuterium and low-triangularity magnetic equilibria ($\delta_{av} = 0.18$–0.22). Fig. 4 shows the time evolution of discharge in JET-ILW with an additional input power of $P_{IN} = P_{NBI} + P_{ICRH} = 15$ MW + 3.1 MW = 18.1 MW performed in two magnetic field shapes. The first part of the discharge is performed in shape A, with the inner strike point on the inner vertical target and the outer one on the horizontal bulk W tile (tile 5). At time 12 s the shape started to change slowly and reached the second magnetic equilibrium (shape B) at t = 12.5 s: the inboard strike point is placed on the inner horizontal tile and the outboard (OSP) on the horizontal row known as tile 6, adjacent to the outboard pumping duct entrance. Poloidal cross-sections of these two magnetic flux contours are shown in Fig. 5a. This plasma discharge reaches a stored energy of 3.5 MJ during the flat top phase with regular type I ELMs with the following characteristics: ELM energy loss of $\Delta W_{ELM} = 0.130$ MJ and an ELM frequency of $f_{ELM} = 35$ Hz. The radiated power is around 6–7 MW throughout the H-mode phase. In Shape B, known as corner configuration with the strike points close to the cryo-pumps, the pumping efficiency of the recycled particles is increased, resulting in a strong modification of the global energy confinement [30]. For a correct comparison of the W screening in the divertor in different magnetic shapes, the global energy confinement, n_e and T_e profiles in the confined region, ELM frequencies as well as the plasma rotation in the core should

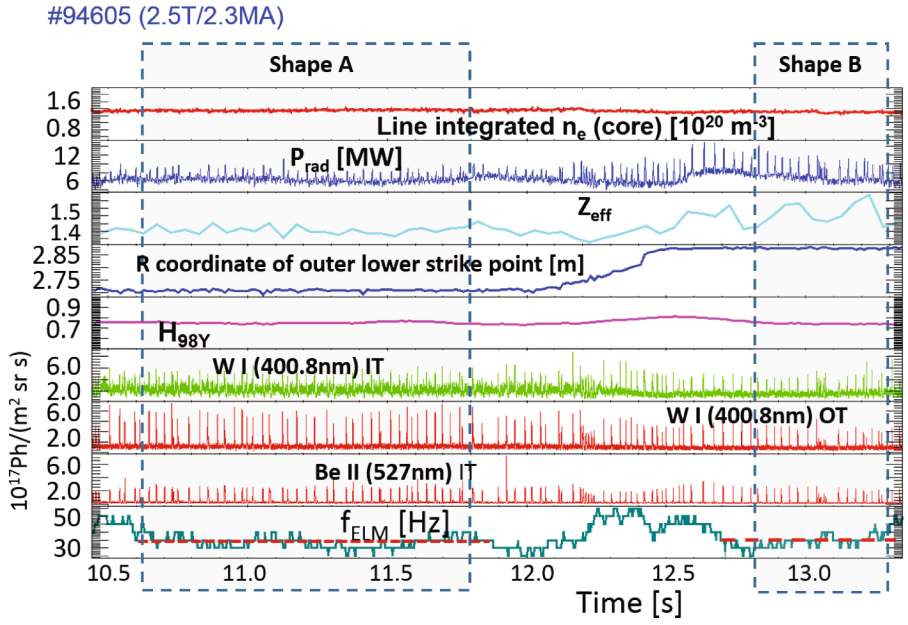

Fig. 4. Time evolution of an H-mode discharge with auxiliary input power of 18.1 MW, a stored energy of 3.5 MJ as well as regular type I ELMs at ELM energy loss of $\Delta W_{ELM} = 0.13$ MJ and ELM frequency of $f_{ELM} = 35$ Hz. At time 12 s the shape was changed slowly and reaches the second magnetic equilibrium (shape B) at t = 12.5 s.

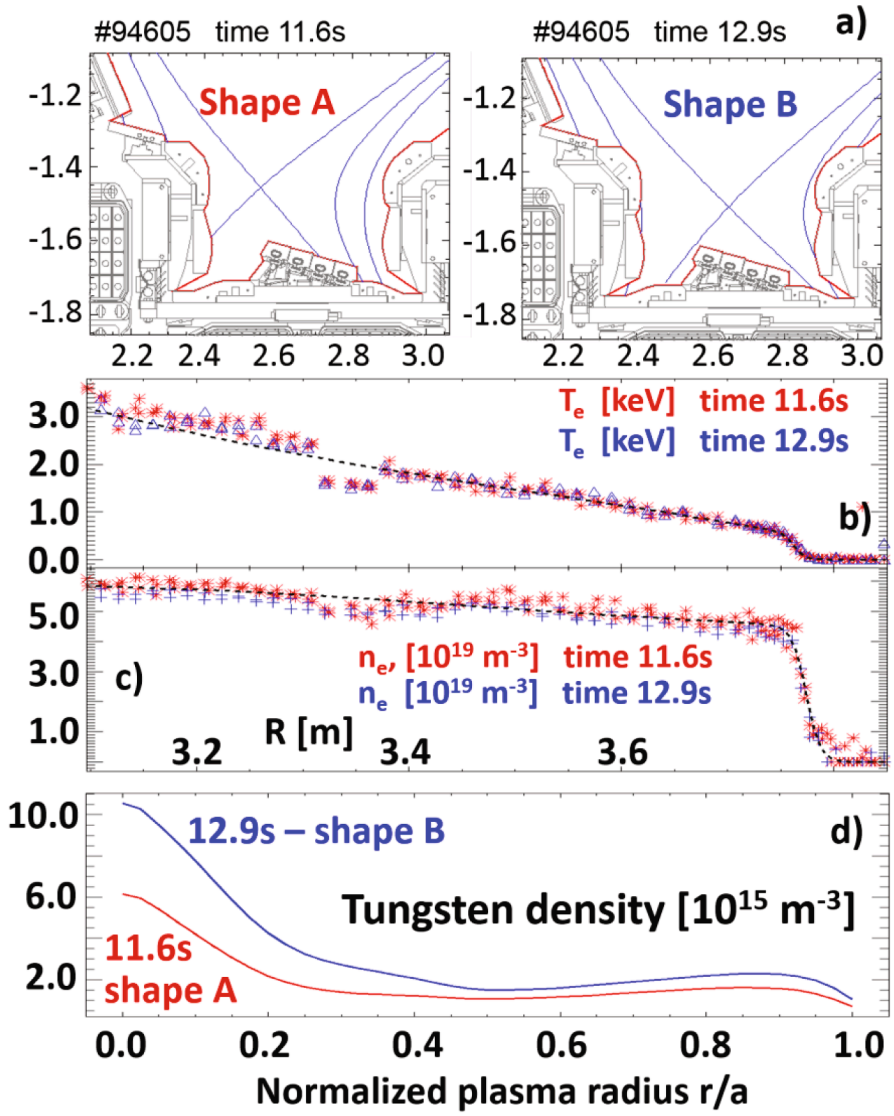

Fig. 5. a) Two plasma shapes, b) n_e and T_e profiles c) tungsten density distributions at the two corresponding time points: 11.6 s [A] and 12.9 s [B].

be kept absolutely identical. Under identical conditions, the global confinement time of the tungsten, τ_W, will be also similar allowing the comparison of S_W by knowing the number of W particles confined in the main plasma, N_W and the tungsten source Γ_W. The adjustment was achieved by increasing the gas fuelling rate during the transition from shape A to B. To avoid H-mode collapse by radiation in the plasma core, a finite D_2 gas rate is required for W control and stable H-mode operation with the ITER-like wall [31]. Therefore, the first phase in shape A is fuelled with a medium D_2 rate of $\approx 4.5 \times 10^{21}$el/s resulting in an ELM frequency of about $f_{ELM} = 35$ Hz. The confinement factor, which gives the energy confinement time with respect to the ITERH98P(y,2) scaling [32], is maintained at a constant level of $H_{98Y} = 0.75$. To keep the H_{98Y} at the same level during the phase with shape B, the fuelling rate is strongly increased up to 3×10^{22}el/s during the shape transition. As a result, both shapes have the same n_e and T_e profiles (Fig. 5b,c at two different times 11.6 s and 12.9 s), $f_{ELM} = 35$ Hz, $H_{98Y} = 0.75$, core plasma rotation with the central velocity of about 100–120 km/s.

Fig. 5b,c demonstrate very identical T_e and n_e profiles at two different times: t = 12.6 s (shape A) and t = 12.9 s (shape B). Because the sawteeth have a significant impact on the W density distribution, these times have been selected at equal distance from the previous crash to keep identical conditions in the comparison. The maximum of the W density in the plasma core ($r/a = 0$) is observed just before the sawtooth crash and the minimum directly after the crash. The role of sawtooth crashes in re-distributing impurities has been intensively discussed in [33].

The W source averaged over five ELMs is evaluated for both phases. The position of the outer strike point in the shape B was chosen so that the W I emission is still visible though the vertical line of sight of the W filterscope diagnostic. Nevertheless, in order to avoid problems with the shadowing of the spectroscopic views, the gross erosion in the outer as well as in the inner divertor has been evaluated by approach (III). As shown in [5], this approach, which is based on the spectroscopic imaging of two digital cameras, collects the entire WI emission (no shadowing of the camera views) and can therefore successfully measure the W erosion in the corner configurations. Please note that in [5] approach (III) was demonstrated for a much deeper corner configuration than in this work. In addition, approach (III) was compared with approach (II), which provided identical results and thus confirmed the correctness of the selected position of the outer strike point. The total sources, which include the gross erosion in the outer as well as in the inner divertor, are $\Gamma_W = 1.2 \times 10^{20}$ atoms/s and $\Gamma_W = 1.12 \times 10^{20}$ atoms/s for the shapes A

and B respectively. Fig. 5d shows the radial distribution of W density evaluated for the compared two shapes. To estimate the 2D poloidal distribution of the intrinsic W density, a newly developed data analysis tool was used [34,35]. The method is based on an integrated approach, searching for an impurity mix that can simultaneously explain the observed soft X-ray emission, the W concentration measured by passive vacuum ultra-violet spectroscopy, the line-of-sight integrated measurement of the effective charge and of the total radiation. The number of W particles confined in the main plasma, $N_{W,}$ can be assessed by:

$$N_W = 4\pi^2 R_0 \kappa \int_0^1 c_W(\rho)\rho d\rho \quad (5)$$

where c_W is the W density and is ρ is the normalized toroidal flux coordinate, $\kappa = b/a$ is plasma elongation, a is the horizontal minor radius and b is the height of the plasma measured from the equatorial plane. The evaluated number of W confined particles in shape A is about $N_W = 1.2 \times 10^{17}$ and is ≈58% lower than in shape B ($N_W = 1.9 \times 10^{17}$ W particles). The increase of the effective charge Z_{eff} of the plasma in shape B from 1.35 to 1.48 is mainly due to the increase in the Be concentration.

Assuming an identical τ_w in plasmas with shape A and B one obtains:

$$S_W{}^A/S_W^B = \left(N_W{}^A/\Gamma_W{}^A\right)/\left(N_W{}^B/\Gamma_W{}^B\right) = 0.59 < 1.0$$

This comparison indicates a better W divertor screening in the case of shape A. Assuming the prompt redeposition fraction is the same in both shapes, the different divertor screening performance in these shapes A and B is probably due to different balance between the thermal force, F_{therm}, and the friction force, F_{fric}, along magnetic field lines. The increased thermal force, induced by the ion and electron temperature gradient, could push the impurity ions up the temperature gradients, dTe,i/dl to the main plasma (core-SOL plasma boundary). Note that the physics of the differences in divertor screening in the studied shapes is not fully understood and detailed modelling in combination with benchmarking on experiments is required. The global particle confinement time τ_W can be determined from the evolution of the core W content during the sudden injection of W particles into the plasma core during the transient impurity events (TIEs). TIEs leading to an unexpected increase in radiated power have been intensively studied in JET from the installation of the ITER-like wall on [36]. Depending on their size, the W particles can reach the plasma confined region resulting in intense radiation spikes. We select TIEs, which were seen in other pulses of our experiments with the identical total heating power and the same H_{98Y}. The TIEs show a clear increase in the W line emissions in the VUV spectral range and the global W confinement time is evaluated by the exponential decay of the total radiation measured by the bolometry system and is τ_W = 130 ms (τ_W is about of the 75% of the energy confinement time $\tau_W \approx 0.75\ \tau_E$). Typically the impurity modulation method has been used as standard method for the determination of the impurity confinement time [37,38]. For example the laser ablation with known impurity species can be used for this purpose [39,40]. The amount of injected impurity into the plasma core should be small enough not to change the global transport. This is a simple method which is very useful for the comparison of the results across the different machines. Here in this work, the TIE (dust particle) event has been used for the determination of the global W particle confinement time. This TIE do not have any impact on the global plasma parameters.

Taking into account the estimated global confinement time for W, the divertor screening factor of W is of about 0.8% and 1.3% for shapes A and B respectively. Thus the screening of the W in the magnetic configuration with strike points on tile 5 is by a factor of about 1.7 more efficient than in the corner configuration with outer strike point at the pumping duct entrance.

It should be noted that the corner configuration is foreseen as reference shape for scenarios of the deuterium–tritium experiments on JET scheduled for 2021.

4. Conclusions

The identification of the tungsten atomic sources has been performed in JET-ILW with the help of optical emission spectroscopy. Three approaches are chosen to provide a quantitative measure of the W-erosion in the outer as well as in the inner divertor regions and to disentangle the erosion source in the intra-ELM phase from the erosion in the inter-ELM phase: it was shown in JET-ILW that the dominant W erosion mechanism in the divertor is the intra-ELM sputtering induced by impurities as well as hydrogenic ions with energies determined by the pedestal temperature. The intra-ELM sputtering prevails by a factor of 7–10 over inter-ELM sputtering in the investigated ELM frequency range from 35 Hz to 80 Hz. The fluence of sputtered tungsten per ELM (atoms/ELM) shows a significant dependence on the ELM frequency. It decreases by a factor of 2.0–2.3 (1.7) with ELM frequency in the outer (inner) divertor. On the other hand, the entire gross erosion W source (the number of eroded W atoms per second) increases with ELM frequencies and reaches its maximum at $f_{ELM} \approx$ 50–55 Hz. Beyond these frequencies, it decreases with the ELM frequency.

The in/out asymmetry of the intra-ELM W sources during ELMs is a critical issue and was investigated in this contribution. Because the recombination emission could strongly affect the measurements of the tungsten emission in the area of the inner divertor, a new algorithm for the subtraction of continuum radiation has been used to evaluate the W erosion in the inner divertor region. It was shown that the contribution of the inner divertor region to the total W source is significant and cannot be neglected. At a lower ELM frequency of about 35 Hz the outer divertor gross W source is larger by a factor of 1.5. However, the in/out asymmetry of the W erosion decreases strongly with ELM frequency demonstrating a nearly symmetric W source in both divertor legs at frequencies above 70 Hz.

Dedicated H-mode experiments have been carried out at JET with the ITER-like wall (JET-ILW) to study the impact of plasma configurations on the divertor tungsten screening. Two different magnetic field shapes -open and closed divertor configuration (corner configuration)- have been analysed. For the comparison, the global energy confinement, n_e and T_e profiles in the confined region, ELM frequencies as well as the plasma rotation in the core were kept absolutely identical in plasmas under both magnetic configurations. The divertor screening factor of W is of about 0.8% and 1.3% for shapes A (open magnetic field configuration) and B (corner configuration) respectively indicating that the magnetic configuration with strike points on tile 5 is more efficient, by a factor about of 1.7, than in the corner configuration with the outer strike point positioned at the pumping duct entrance.

Declaration of Competing Interest

The authors declare that they have no known competing financial interests or personal relationships that could have appeared to influence the work reported in this paper.

Acknowledgement

This work has been carried out within the framework of the EUROfusion Consortium and has received funding from the Euratom research and training programme 2014-2018 and 2019-2020 under grant agreement No 633053. The views and opinions expressed herein do not necessarily reflect those of the European Commission.

References

[1] S. Brezinsek, et al., Nucl. Fusion 59 (2019), 096035.
[2] G.J. van Rooij, et al., J. Nucl. Mater. 438 (2013) S42.
[3] R. Dux, et al., J. Nucl. Mater. 390–391 (2009) 858–863.
[4] N. Den Harder, et al., Nucl. Fusion 56 (2016), 026014.
[5] A. Huber, et al., Nucl. Mater. Energy 18 (2019) 118–124.

[6] A. Meigs, M. Stamp, R. Igreja, S. Sanders, P. Heesterman, Rev. Sci. Instrum. 81 (2010), 10E532.
[7] B.A. Lomanowski et al., Nucl. Fusion 55 (2015) 123028 (14pp).
[8] P.D. Morgan, K.H. Behringer, P.G. Carolan, M.J. Forrest, N.J. Peacock, M.F. Stamp, Rev. Sci. Instrum. 56 (1985) 862–864.
[9] A. Huber, et al., Rev. Sci. Instrum. 83 (2012) 10D511.
[10] A. Huber, et al., Fusion Eng. Des. 88 (2013) 1361–1365.
[11] M. Laengner, et al., J. Nucl. Mater. 438 (2013) S865.
[12] S. Brezinsek, et al., Phys. Scr. T170 (2017), 014052.
[13] H. P. Summers et al., Atomic Data and Analysis Structure, URL: http://www.adas.ac.uk/.
[14] T. Abrams, et al., Nucl. Mater. Energy 17 (2018) 164.
[15] Ch. Guillemaut, et al., Plasma Phys. Control. Fus. 57 (2015), 085006.
[16] A. Loarte et al. 11 (2004) Physics of Plasmas, 2668; https://doi.org/10.1063/1.1707025.
[17] E. Solano et al., Effect of fuelling location on pedestal and ELMs in JET, Proceedings of 41st EPS Conference on Plasma Physics.
[18] A. Loarte, et al., Plasma Phys. Control. Fusion 45 (2003) 1549.
[19] A. Hermann, Plasma Phys. Contr. Fusion 44 (2002) 883.
[20] T. Abrams, et al., Phys. Plasmas 26 (2019), 062504, https://doi.org/10.1063/1.5089895.
[21] A. Kirschner, et al., Nucl. Mater. Energy 18 (2019) 239–244.
[22] D. Moulton, et al., Plasma Phys. Control. Fus. 55 (2013), 085003.
[23] Ch. Guillemaut, et al., Nucl. Fusion 58 (2018), 066006, https://doi.org/10.1088/1741-4326/aab7b1.
[24] I. Borodkina, et al., Nucl. Mater. Energy 12 (2017) 341.
[25] W. Eckstein et al., Report IPP 9/132 (2002).
[26] P.C. Stangeby, The Plasma Boundary of Magnetic Fusion Devices, Institute of Physics Publishing, Bristol, 2000.
[27] G. Fussmann et al 1995 Plasma Physics and Controlled Nuclear Fusion Research 1995 (Proc. 15th Int. Conf. (Seville 1995)) vol 2 (Vienna: IAEA)].
[28] D. Naujoks, et al., Nucl. Fusion 36 (1996) 671.
[29] K. Krieger, et al., J. Nucl. Mater. 266–269 (1999) 207.
[30] E. Joffrin, et al., Nucl. Fusion 57 (2017), 086025.
[31] E. Joffrin, et al., Nuclear Fusion 54 (1) (2014), 013011.
[32] ITER Physics Expert Group on Confinement, Transport, ITER Physics Expert Group on Confinement Modelling, Database and ITER Physics Basis Editors 1999 Chapter 2.
[33] M. F.F. Nave et all Nucl. Fusion 43 (2003) 1204–1213.
[34] M. Sertoli, et al., Rev. Sci. Instrum. 89 (2018), 113501.
[35] M. Sertoli, et al., J. Plasma Phys. 85 (2019) 905850504.
[36] M. Sertoli et al., Phys. Scr. T159 (2014) 014014 (4pp).
[37] W.K. Leung, et al., Plasma Phys. Control. Fusion 28 (1986) 1753.
[38] J. Castracane, et al., Nucl. Fusion 27 (1987) 1921.
[39] D. Pasini, et al., Nuclear Fusion 30 (1990) 2049.
[40] D. Pasini, et al., Plasma Phys. Control. Fus. 34 (1992) 677.